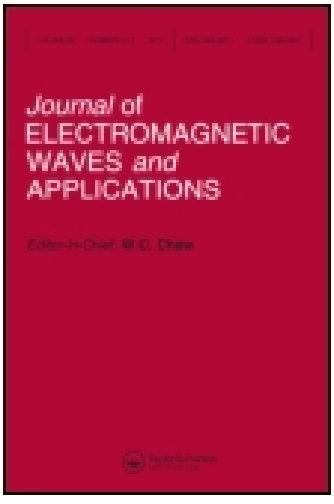

Journal of Electromagnetic Waves and Applications

Publication details, including instructions for authors and subscription information:
http://www.tandfonline.com/loi/tewa20

A Quadrature Algorithm for the Evaluation of a 2d rAdiation Integral With a Highly Oscillating Kernel

R. Borghi [a] , F. Frezza [b] , M. Santarsiero [c] , C. Santini [d] & G. Schettini [e]

[a] Dip. di Ingegneria Elettronica, Università Roma Tre and INFM Via della Vasca Navale 84, I-00146 Rome, Italy

[b] Dip. di Ingegneria Elettronica, Università La Sapienza Via Eudossiana 18, I-00184 Rome, Italy

[c] Dip. di Fisica, Università Roma Tre and INFM Via della Vasca Navale 84, I-00146 Rome, Italy

[d] Telecom Italia Direzione Generale, Rome, Italy

[e] Dip. di Ingegneria Elettronica, Università Roma Tre Via della Vasca Navale 84, I-00146 Rome, Italy

Published online: 03 Apr 2012.

To cite this article: R. Borghi , F. Frezza , M. Santarsiero , C. Santini & G. Schettini (2000) A Quadrature Algorithm for the Evaluation of a 2d rAdiation Integral With a Highly Oscillating Kernel, Journal of Electromagnetic Waves and Applications, 14:10, 1353-1370, DOI: 10.1163/156939300X00121

To link to this article: http://dx.doi.org/10.1163/156939300X00121

Journal of Electromagnetic Waves and Applications, Vol. 14, 1353–1370, 2000

A QUADRATURE ALGORITHM FOR THE EVALUATION OF A 2D RADIATION INTEGRAL WITH A HIGHLY OSCILLATING KERNEL

R. Borghi

Dip. di Ingegneria Elettronica, Università Roma Tre and INFM
Via della Vasca Navale 84, I-00146 Rome, Italy

F. Frezza

Dip. di Ingegneria Elettronica, Università La Sapienza
Via Eudossiana 18, I-00184 Rome, Italy

M. Santarsiero

Dip. di Fisica, Università Roma Tre and INFM
Via della Vasca Navale 84, I-00146 Rome, Italy

C. Santini

Telecom Italia
Direzione Generale, Rome, Italy

G. Schettini

Dip. di Ingegneria Elettronica, Università Roma Tre
Via della Vasca Navale 84, I-00146 Rome, Italy

Abstract–The general solution of the 2D electromagnetic scattering problem may be expressed in terms of the so called Cylindrical Waves [4]. In the presence of a plane discontinuity, the solution of the electromagnetic problem may be found by means of the plane-wave expansion of the Cylindrical Waves and by characterizing the discontinuity by means of the reflection coefficient. In this way a numerical solution implies the quadrature of 2D radiation integrals with a highly oscillating kernel, to be solved by means of special quadrature algorithms. In

particular, to achieve accurate and fast computation, a special adaptive Gauss-Kronrod quadrature algorithm has been developed. Numerical stability and accuracy tests are presented.

1. INTRODUCTION

The general solution of the two-dimensional electromagnetic problem may be expressed in terms of the so-called Cylindrical Waves, depending on the cylindrical coordinates ρ, ϑ and defined as

$$CW_n(\rho, \vartheta) = H_n(\rho)\, e^{in\vartheta}, \tag{1}$$

where ρ is a normalized radius and H_n denotes the first type Hankel function [1]. Since these functions are the eigenfunctions of the two dimensional Laplace operator they can be assumed as a basis for describing solutions of the two dimensional electromagnetic problem, constituted by the Helmholtz equation with the Sommerfeld radiation condition.

In the presence of a plane surface, a solution may be found by means of a plane-wave expansion of the incident and diffracted fields provided that we take into account the influence of the plane discontinuity by characterizing it with a reflection coefficient $\Gamma(\beta)$ where β is the wavevector component parallel to the surface. The so-called diffracted-reflected field, i.e., the field diffracted by the conducting cylinders and reflected by the surface, may be expressed as a series of Reflected Cylindrical Waves $\mathrm{RW}_n(\xi, \zeta)$ defined as follows:

$$\mathrm{RW}_n(\xi, \zeta) = \frac{1}{2\pi} \int_{-\infty}^{+\infty} \Gamma(\beta)\, F_n(\xi, \beta)\, e^{i\beta\zeta} d\beta, \tag{2}$$

where the normalized rectangular coordinates ξ and ζ have been used; the $F_n(\xi, \beta)$ functions may be expressed in a compact form given in [2]. In Eq. (2) the RW_n functions are defined by their plane-wave expansion and in general, for an arbitrary $\Gamma(\beta)$ function, must be numerically evaluated. This approach has been applied to the study of Quasi-Optical Grills for thermonuclear plasma heating [3]. To this aim, quite complex structures must be simulated: this implies the numerical evaluation of a large amount of integrals in the form of Eq. (2). A numerical study of the integral representation of the RW_n functions has been presented in [4] and good numerical results have been achieved

by developing special integration procedures. In this paper we give a detailed description of the numerical method we developed to achieve accurate and speedy numerical integration of the homogeneous spectrum of the RW_n functions, i.e., the integral in Eq. (2) in the range $\beta \in [-1, 1]$,

$$I_n^{\text{int}}(\xi, \zeta) = \int_{-1}^{+1} \Gamma(\beta) \frac{e^{i\left(\xi\sqrt{1-\beta^2} - n \arccos\beta + \beta\zeta\right)}}{\sqrt{1-\beta^2}} d\beta. \tag{3}$$

With a little algebra it is possible to show that:

$$I_n^{\text{int}}(\xi, \zeta) = \mathcal{I}_n^{\text{int}}(\rho, \vartheta) = \frac{1}{\pi} \int_0^{\pi} \Gamma(\cos t)\, e^{i[\rho \sin(t+\vartheta) - nt]} dt. \tag{4}$$

Thus, the special integration method we developed may be used as an efficient algorithm for the numerical evaluation of the following kind of integrals:

$$I_n(\rho, \vartheta) = \int_0^{\pi} \Gamma(\cos t)\, e^{i[\rho \sin(t+\vartheta) - nt]} dt. \tag{5}$$

2. INTEGRATION ALGORITHM

Difficulties arise from the highly oscillating character of the integrand for values $\rho \gg 1$ and $n \gg 1$, since the term $e^{i[\rho \sin(t+\vartheta)]}$ behaves like a polynomial function whose degree depends on the two parameters ρ and ϑ. In particular the number of zeros of the integrand increases as a direct function of the term $(\rho - \vartheta)$. Two examples of plots of the real and imaginary parts of the integrand are given in Fig. 1 and Fig. 2. Further difficulties arise from the presence of the arbitrary function $\Gamma(\cos t)$, which depends on the kind of interface chosen. Integration of rapidly oscillating functions has been faced with different approaches by many authors [5]: in this particular case, the severe specifications for integration speed and accuracy of the numerical value led us to develop a special integration algorithm.

Numerical tests carried out by taking into account several different expressions of the $\Gamma(\cos t)$ function have shown that the employment of elementary integration rules (such as the Trapezoidal or Simpson's rule) implies a very slow convergence, thus suggesting the adoption

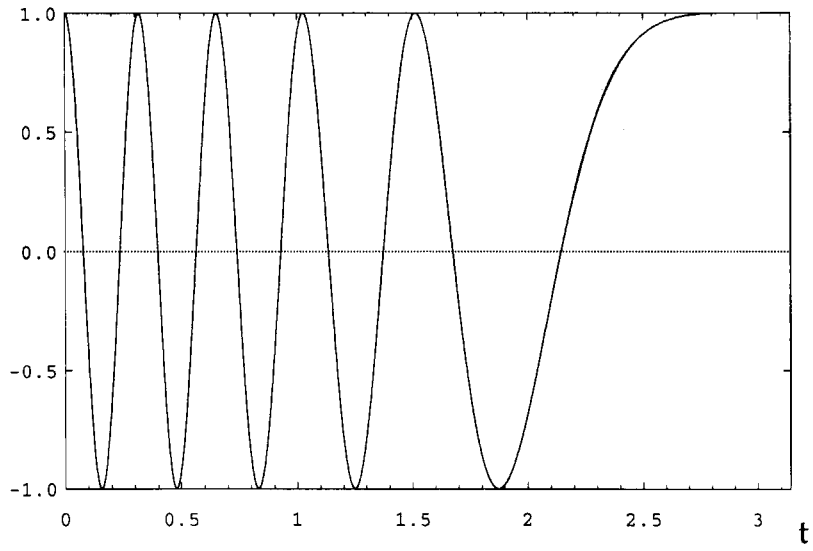

Figure 1. Plot of the real part of the integrand, i.e., $g(t) = \Gamma(\cos t) \cos[\rho \sin(t + \vartheta) - nt]$ in the case $\Gamma(\cos t) = 1$, $\rho = 10$, $\vartheta = 0$, $n = -10$.

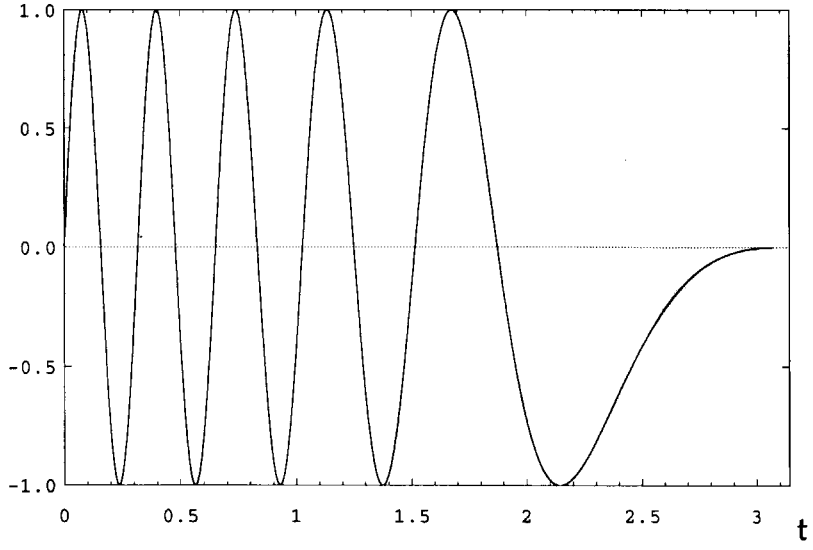

Figure 2. Plot of the imaginary part of the integrand, i.e., $g(t) = \Gamma(\cos t) \sin[\rho \sin(t + \vartheta) - nt]$ in the case $\Gamma(\cos t) = 1$, $\rho = 10$, $\vartheta = 0$, $n = -10$.

of Gaussian quadrature rules. Since the number of oscillations of the integrand does not reach an upper bound for $\rho, m \to \infty$, it is not possible to fix the maximum order of the Gaussian rule to be adopted. By increasing, step by step, the order of the quadrature formula, it is not possible to obtain a fast convergence to the desired accuracy.

To overcome such problems, we adopted a generalized Gaussian integration method, consisting in a decomposition of the integration interval in subintervals of suitable length on which a fixed low-order Gaussian rule gives good accuracy. Thus, the problem of *a priori* choice of the minimum order to obtain a desired accuracy turns into the problem of finding a decomposition of the integration domain which leads to the best results with minimum computational weight. By decomposing $[0, \pi]$ in equal subdomains of fixed width, it is difficult to find an efficient solution: in fact, by choosing the fixed subinterval width equal to the minimum distance in between two consecutive zeroes of the integrand, we get too fine a mesh and long computational time; by choosing the average distance in between two zeros as fixed subinterval width, we get losses of accuracy in all subintervals where the oscillatory behavior is higher. We point out that carrying out an integration algorithm optimization based on the kernel oscillatory behaviour alone, does not avoid possible accuracy losses due to perturbations introduced by the $\Gamma(\cos t)$ function.

A suggested way to achieve such decomposition [5], consists in choosing as subinterval bounds the zeros of the integrand. Nevertheless, following this procedure a big number of roots must be determined by using numerical methods. Here we present a method for avoiding the numerical search of all those roots. In fact, the apparently irregular behaviour of the integrand can be understood by separating the oscillating Kernel in its real and imaginary parts, as follows:

$$e^{i[\rho \sin(t+\vartheta)-nt]} = \cos[\rho \sin(t+\vartheta) - nt] + i \sin[\rho \sin(t+\vartheta) - nt]. \quad (6)$$

The Kernel is now expressed as a linear superposition of circular functions of argument $\rho \sin(t+\vartheta) - nt$, i.e., trigonometric functions whose argument is nonlinear and is a periodic function as well: these functions are related with frequency modulated electric signals. For an elementary trigonometric function, such as

$$g(t) = \cos(\omega t + \varphi_0), \quad (7)$$

where ω is the angular frequency, the frequency f and the period T

are defined as follows:

$$f = \frac{\omega}{2\pi}, \qquad T = \frac{1}{f}. \tag{8}$$

We prefer to use the term "oscillation rate" instead of the term frequency to avoid ambiguity. In case of functions like in Eq. (6), the oscillation rate is not a constant. In fact, for a function of the kind

$$g(t) = \cos\left[\varphi(t)\right], \tag{9}$$

the local oscillation rate $f(t)$ is defined as

$$f(t) = \left| \frac{1}{2\pi} \frac{d\varphi(t)}{dt} \right|. \tag{10}$$

A function of the kind in Eq. (6) has the following oscillation rate:

$$f(t) = \frac{1}{2\pi} \left| \frac{d}{dt} \left[\rho \sin\left(t + \vartheta\right) - nt\right] \right| = \frac{1}{2\pi} \left|\rho \cos\left(t + \vartheta\right) - n\right|. \tag{11}$$

In Figs. 3(a) and 3(b) the integrand is represented together with the $f\,(t)$ function: it is possible to note that the oscillation rate function assumes greater values in all points of $[0, \pi]$ where oscillations are steeper; in all the points where the oscillation rate function has a zero, the integrand has a smooth behaviour and shows an extremum. The definition of local oscillation rate given in Eq. (10) allows us to obtain an efficient decomposition of the $[0, \pi]$ domain by choosing the width of the generic subinterval as proportional to the average value of the local oscillation period. Furthermore, a simple algorithm has been developed to estimate such average value. The consequent generalized Gaussian quadrature rule is based on an integration interval decomposition with a variable number of subdomains depending on the oscillatory behaviour of the integrand: the mesh is refined in all points where the integrand undergoes rapid variations. Therefore, the proposed integration algorithm is an adaptive one. To describe the algorithm used to choose the generic subinterval width, we refer to Fig. 3 in which the imaginary part of the integrand is shown for a particular choice of the parameters. As an example, we applied the algorithm starting from one of the roots of the integrand function,

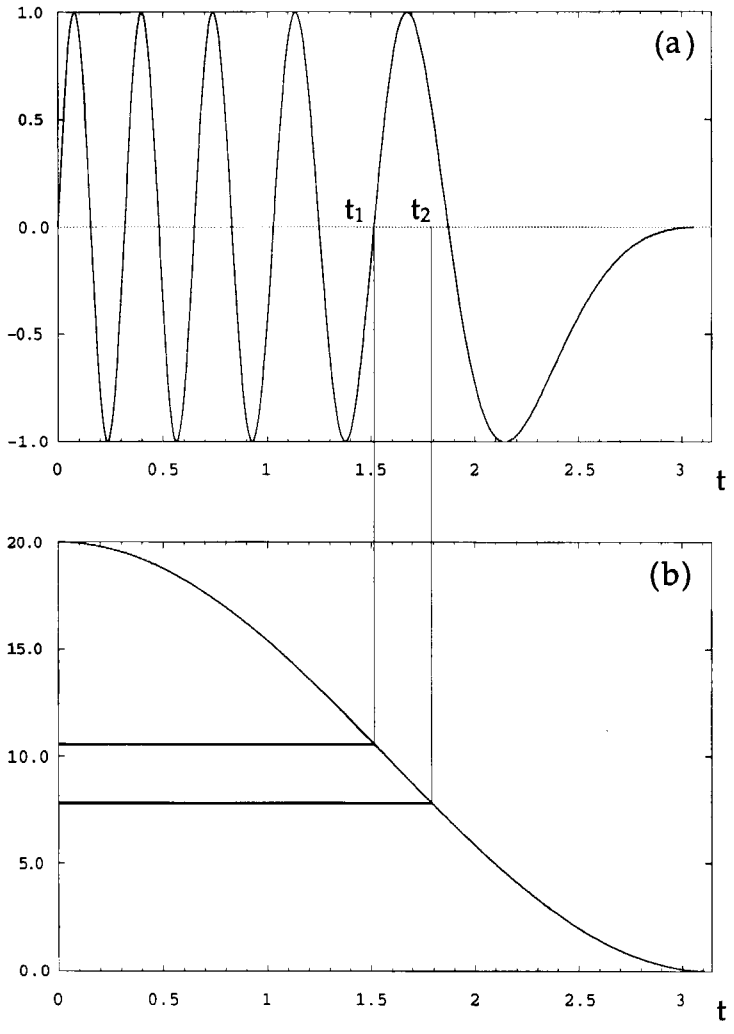

Figure 3. (a) Plot of the imaginary part of the integrand in the same case as in Fig. 2, i.e., $g(t) = \Gamma(\cos t) \sin[\rho \sin(t + \vartheta) - nt]$ in the case $\Gamma(\cos t) = 1$, $\rho = 10$, $\vartheta = 0$, $n = -10$. (b) Plot of the oscillation rate function $f(t) = \frac{1}{2\pi} |\rho \cos(t + \vartheta) - n|$ corresponding to the function in Fig. (a), i.e., in the case $\rho = 10$, $\vartheta = 0$, $n = -10$; $t_1 = \pi/2$ is one of the roots of the $g(t)$ function; $t_2 = t_1 + \frac{1}{f(t_1)}$ is a defective approximation of the next root as explained in the text.

namely $t = t_1 = \pi/2$. We define the effective oscillation period as the quantity $T_{\text{eff}}(t)$ for which

$$g(t_1) = g\left[t_1 + T_{\text{eff}}(t_1)\right], \tag{12}$$

where $g(t_1)$ is the real or the imaginary part in Eq. (6). Note that the unknown value T_{eff} depends on the value t_1 because $g(t)$ is not strictly periodic. In this example t_1 is a zero of the $g(t)$ function, so we define the new abscissa t' as

$$t' = t_1 + T_{\text{eff}}\left(t_1\right). \tag{13}$$

Owing to Eq. (12) t' is still a zero of the integrand and, as we explained before, is the upper bound of an optimized integration subinterval $[t_1, t']$. Since the value T_{eff} is not available, an algorithm for its estimation must be used. We use the following algorithm:

1. We evaluate the local oscillation rate in the initial point t_1, as defined in Eqs. (10) and (11)

$$f(t_1) = \frac{1}{2\pi}\left|\rho\cos\left(t_1 + \vartheta\right) - n\right| = f_1. \tag{14}$$

2. We evaluate the first approximation of T_{eff} in t_1 as

$$T_1 = \frac{1}{f_1}. \tag{15}$$

3. We evaluate the abscissa $t_2 = t_1 + T_1$. It is possible to note in Fig. 3 that f_1 is the highest value of $f(t)$ in the interval $[t_1, t_2]$. Thus, T_1 is a defective approximation of the effective oscillation period T_{eff}

$$T_1 < T_{\text{eff}}. \tag{16}$$

4. We evaluate the local oscillation rate in t_2

$$f(t_2) = \frac{1}{2\pi}\left|\rho\cos\left(t_2 + \vartheta\right) - n\right| = f_2. \tag{17}$$

5. We evaluate a second approximation of $T_{\text{eff}}(t_1)$ as

$$T_2 = \frac{1}{f_2}. \tag{18}$$

It is possible to note in Fig. 3 that f_2 is the lowest value of $f(t)$ in the interval $[t_1, t_2]$. Thus, T_2 is an excess approximation of the effective oscillation period T_{eff}

$$T_2 > T_{\text{eff}}. \tag{19}$$

6. As approximate value of $T_{\text{eff}}(t_1)$, we choose the average of T_1 and T_2; we name it mean oscillation period $\bar{T}$

$$\bar{T} = \frac{T_1 + T_2}{2}. \tag{20}$$

The integration subinterval with t_1 as lower bound is then chosen as proportional to the mean oscillation period, that is

$$[t_1, t_1 + \alpha\bar{T}], \tag{21}$$

where α is a suitable positive parameter. In practice, this means that α influences the number of oscillations contained in each subinterval. In order to use low-order quadrature formulas, α must be sufficiently small, typically less than one. On the other hand, if α is too small, the number of subintervals may be too large, so that a compromise has to be found for the choice of α. The next step is to choose the abscissa $t_1 + \bar{T}$ as lower bound of the next subinterval. The algorithm must be applied again until a complete decomposition of the integration domain $[0, \pi]$ is achieved. Depending on the values of the ρ, ϑ, and n parameters, the local oscillation rate function $f(t)$ could present some extrema within the $[0, \pi]$ interval. Nevertheless, for a better performance of the algorithm, it is useful to make a decomposition of the whole interval in the union of subintervals in which the $f(t)$ function behaves monotonically.

Once such a decomposition has been carried out, we still have to specify the order of the Gaussian quadrature rule to be applied on each subdomain. A simple low-order Gauss-Legendre rule gives good results in many cases but is not able to avoid a possible local accuracy loss on those subintervals in which the $\Gamma(\cos t)$ function perturbates the oscillating Kernel in a significant way. A limitation for the global error of the Gaussian rule on the whole integration interval may be achieved by limiting the single error of the low-order quadrature rule applied on each subdomain. To this aim, the Gauss-Kronrod rule [5] turns out to be extremely useful. By means of this rule, it is possible to estimate

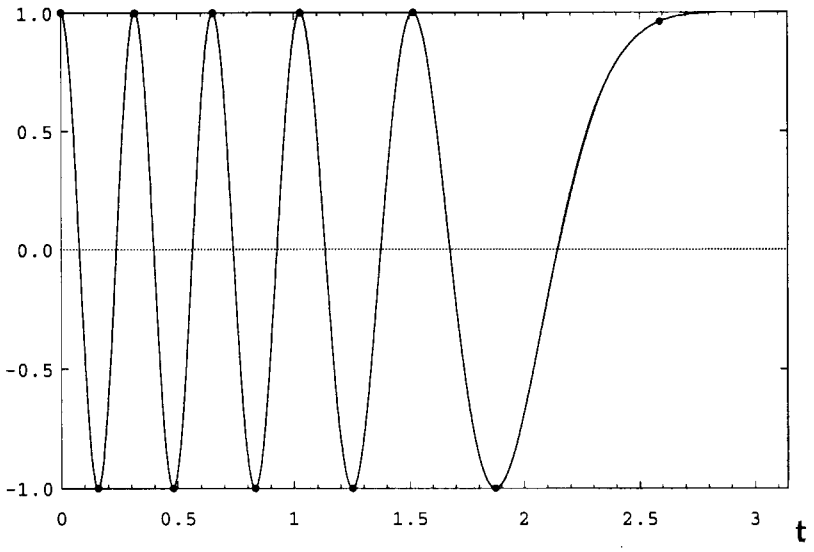

Figure 4. Plot of the real part of the integrand, i.e., $g(t) = \Gamma(\cos t) \cos[\rho \sin(t + \vartheta) - nt]$ in the case $\Gamma(\cos t) = 1$, $\rho = 10$, $\vartheta = 0$, $n = -10$. Dots show the values of the $g(t)$ function on the adaptive decomposition subinterval endpoints.

the numerical accuracy achieved on each subinterval with a negligible increase of the computational time. In those cases in which the desired accuracy is not achieved, a recurrent mesh refinement procedure is applied, by which the subinterval under analysis undergoes a further decomposition.

2.1 Results of the Adaptive Integration Rule

The adaptive algorithm for the decomposition of the integration domain revealed fairly efficient for a wide range of values for ρ, ϑ, and n. In the following, results are shown for the integrands plotted in Figures 1 and 2, where the parameter α [see Eq. (21)] has been chosen as $1/2$. In Fig. 4 the real part of the integrand in Fig. 1 is shown together with the end points of the subintervals in which $[0, \pi]$ has been decomposed. The adaptive algorithm has found at the start point $t = 0$ a maximum of the integrand and, by tracking the subsequent oscillations, has chosen as subinterval endpoints all the integrand extrema in $[0, \pi]$. In Fig. 5 the imaginary part of the integrand in Fig. 2 is shown

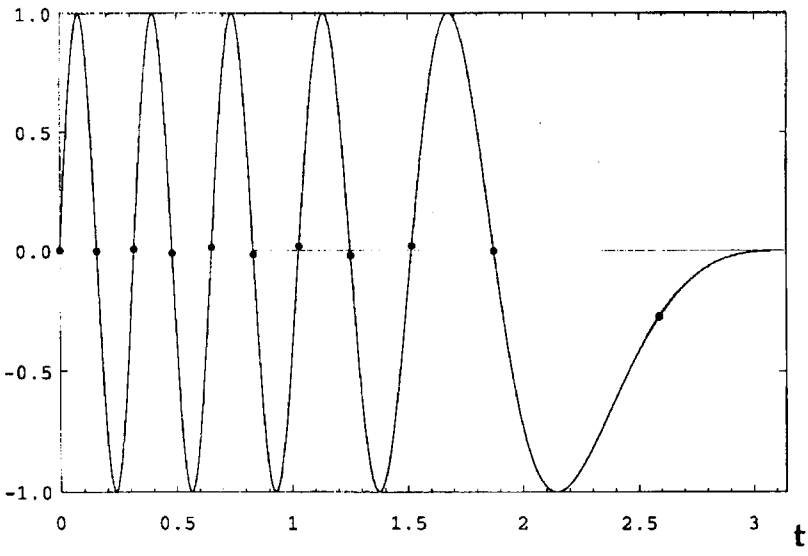

Figure 5. Plot of the imaginary part of the integrand, i.e., $g(t) = \Gamma(\cos t)\sin[\rho\sin(t+\vartheta) - nt]$ in the case $\Gamma(\cos t) = 1$, $\rho = 10$, $\vartheta = 0$, $n = -10$. Dots show the values of the $g(t)$ function on the adaptive decomposition subinterval endpoints.

together with its subinterval end points. It is possible to notice that the adaptive algorithm, starting from the point $t = 0$, first zero of the integrand, has been able to track all subsequent zeros. In both cases, an adaptive integration domain decomposition has been achieved.

In Fig. 6 the real part of the integrand in Fig. 1 is shown together with its subinterval end points. The number of oscillations of the integrand has greatly increased owing to the higher values of ρ and ϑ parameters, but the adaptive algorithm is able to track them anyway. Narrower subintervals are used in those points where the integrand has no regular behaviour while wider subintervals are used where the integrand is smoother. In Fig. 7 the imaginary part of the integrand in Fig. 2 is shown together with its subinterval end points.

3. NUMERICAL RESULTS

In this section we present the results of numerical accuracy and stability tests for the adaptive Gauss-Kronrod integration routines we developed. To this aim it is possible to see that Eq. (5) turns into the

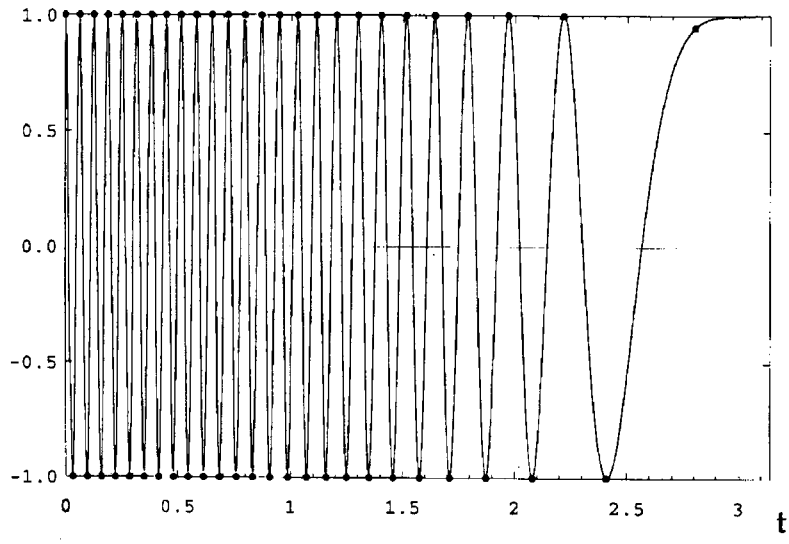

Figure 6. Plot of the same function as in Fig. 4 in the case $\Gamma(\cos t) = 1,\ \rho = 50,\ \vartheta = 0,\ n = -50$.

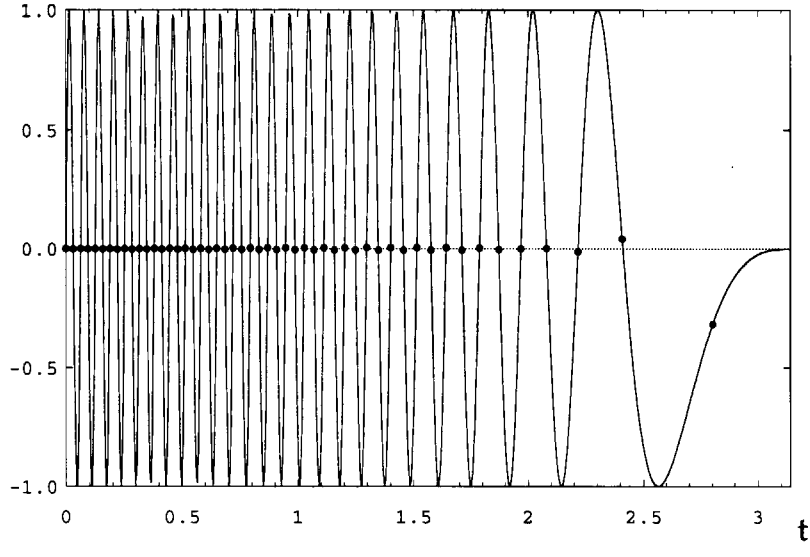

Figure 7. Plot of the same function as in Fig. 5 in the case $\Gamma(\cos t) = 1,\ \rho = 50,\ \vartheta = 0,\ n = -50$.

integral representation of the $J_n(\rho)$ Bessel function of n^{th} integer order by posing $\vartheta = 0$ and $\Gamma(\cos t) = 1$.

$$\mathcal{I}_n^{\text{int}}(\rho, 0) = \int_0^{\pi} e^{i[\rho \sin(t) - nt]} dt = \pi J_n(\rho). \tag{22}$$

As well known, an accurate evaluation of the $J_0(\rho)$, $J_1(\rho)$ Bessel functions may be easily carried out by means of the 20^{th} order polynomial approximation given in [1], while the generic $J_n(\rho)$ Bessel function of n^{th} integer order may be approximated by using a recurrence relation involving $J_0(\rho)$ and $J_1(\rho)$ as described in [6].

Thus, a simple way to test the numerical accuracy and stability of the adaptive integration routines is evaluating the $J_n(\rho)$ Bessel function for a wide range of values for ρ by means of Eq. (22) and comparing such approximation with the results given by the use of the polynomial expansion and recurrent relation. We define an Absolute Error function $E_n(\rho)$ as

$$E_n(\rho) = \left| J_n^{int}(\rho) - J_n^{pr}(\rho) \right|, \tag{23}$$

where $J_n^{int}(\rho)$ represents the approximation of the $J_n(\rho)$ Bessel function of n^{th} integer order given by the integration of Eq. (22), whereas $J_n^{pr}(\rho)$ is the approximation of the $J_n(\rho)$ Bessel function given by the recurrent relation involving $J_0(\rho)$ and $J_1(\rho)$.

In Figs. 8–11 the Absolute Error Function referring to $J_0(\rho)$, $J_5(\rho)$, $J_{10}(\rho)$, $J_{15}(\rho)$ is plotted in the range $\rho \in [1, 10^4]$, showing accuracy and stability in the integral representation of the Bessel functions even for large orders and abscissas.

We stress that the adaptive Gauss-Kronrod routine has been developed for the integration of Eq. (5) in those cases in which the $\Gamma(\cos t)$ function, far from being a constant, represents the reflection coefficient of the plane discontinuity. In particular, in [3] the evaluation of Eq. (5) involved in the computation of the Reflected Cylindrical Waves has been faced for a vacuum-plasma discontinuity with an increasing plasma density. In such case, the irregular behaviour of the Γ function makes an adaptive routine recommendable in order to reduce local integration accuracy loss due to steep variation of the integrand.

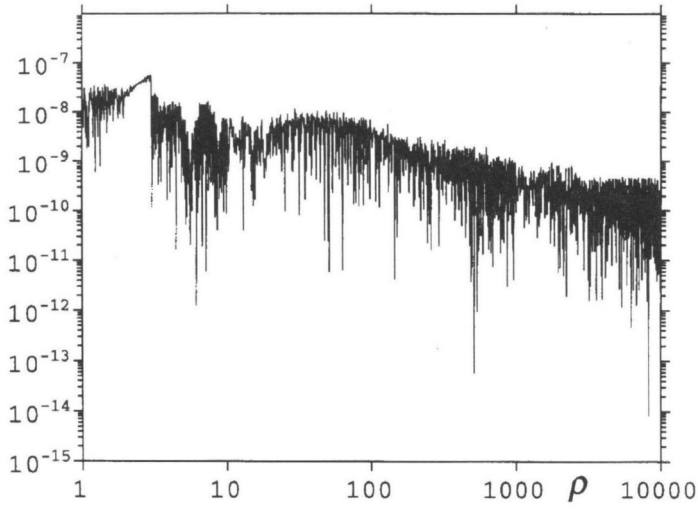

Figure 8. Plot of the absolute error function $E_0(\rho)$ in the range $\rho = [1, 10^4]$.

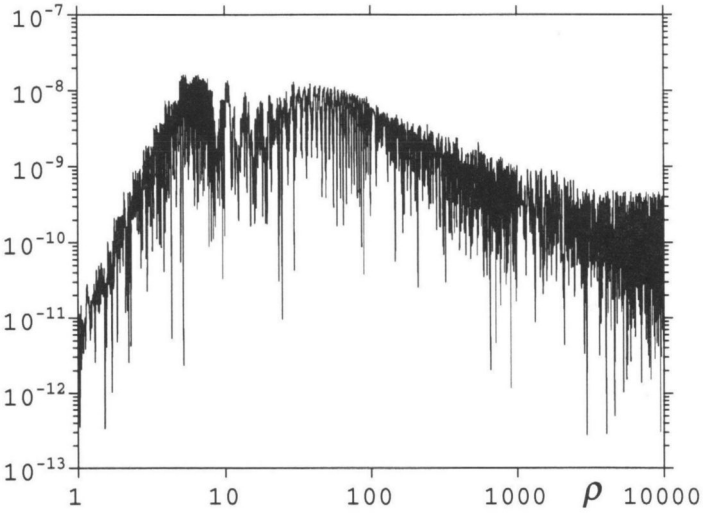

Figure 9. Plot of the absolute error function $E_5(\rho)$ in the range $\rho = [1, 10^4]$.

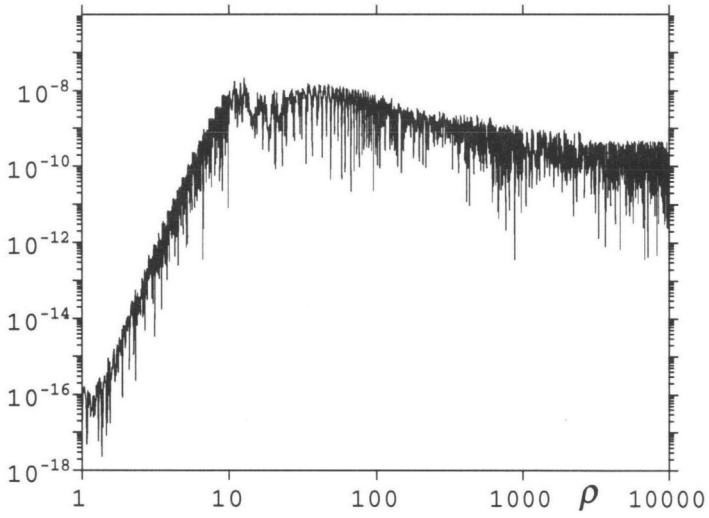

Figure 10. Plot of the absolute error function $E_{10}(\rho)$ in the range $\rho = [1, 10^4]$.

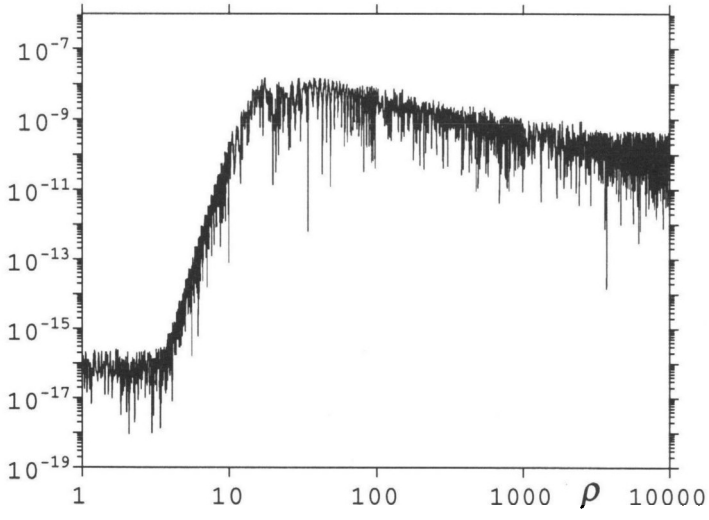

Figure 11. Plot of the absolute error function $E_{15}(\rho)$ in the range $\rho = [1, 10^4]$.

4. CONCLUSIONS

In this paper we present an efficient adaptive algorithm for the integration of the homogeneous plane-wave spectrum resulting from the reflection of a Cylindrical Wave on an infinite plane interface between free space and a generic substrate. The numerical technique we developed may be used for the quadrature of a class of 2D diffraction integrals involving a generic function (the Γ reflection coefficient characterizing the plane interface) modulated by a particular highly oscillating kernel. The numerical solution of the diffraction integral is achieved by carrying out a special adaptive decomposition of the integration domain and by applying a Gauss-Kronrod quadrature rule on each sub-domain of the decomposition. In this way it is possible to achieve a limitation of the global error of the Gaussian rule by checking possible accuracy losses on each sub-domain, even in those cases in which the modulated function has an irregular behaviour. Numerical accuracy and stability of the integration technique is tested in a particular case in which a closed-form solution of the integral is possible. The algorithm has been applied in the numerical study of Cylindrical Wave reflection on a vacuum-dielectric and vacuum-plasma plane interface as shown in [4] and further applications may result by adapting such numerical technique to the solution of diffraction integrals of similar form.

REFERENCES

1. Abramowitz, M., and I. Stegun, *Handbook of Mathematical Functions,* Dover Publications, New York, 1972.
2. Borghi, R., F. Frezza, F. Gori, M. Santarsiero, and G. Schettini, "Plane-wave scattering by a perfectly conducting circular cylinder near a plane surface: cylindrical-wave approach," *J. Opt. Soc. Am. A,* Vol. 13, 483–493, 1996.
3. Borghi, R., F. Frezza, G. Gerosa, M. Santarsiero, C. Santini, and G. Schettini, "Quasi-optical grill launching of lower-hybrid waves for a linearly increasing plasma density," *IEEE Trans. Plasma Science,* Vol. 26, 1330–1338, 1998.
4. Borghi, R., F. Frezza, M. Santarsiero, C. Santini, and G. Schettini, "Numerical study of the reflection of cylindrical waves by a generally reflecting flat surface," *J. Electromag. Waves Appl.,* Vol. 13, 27–50, 1999.
5. Davis, P., and P. Rabinowitz, *Methods for Numerical Integration,* Academic Press, New York, 1984.

6. Press, W. H., W. T. Vetterling, S. A. Teukolsky, and B. P. Flannery, *Numerical Recipes in Fortran 77: The Art of Scientific Computing,* 2nd edition, Cambridge University Press, 1992.

Riccardo Borghi received the *Laurea* degree in Electronic Engineering in 1991 and the Ph.D. degree in Applied Electromagnetics in 1997, from "La Sapienza" University of Rome. In 1997 he joined the Department of Electronic Engineering of University "Roma Tre". His main interests are laser beam propagation, diffractive optics, scattering of electromagnetic and acoustic waves.

Fabrizio Frezza received the *Laurea* degree *cum laude* in Electronic Engineering from 'La Sapienza' University of Rome, Italy, in 1986. In 1991 he obtained the Doctorate in applied electro-magnetics from the same university. In 1986, he joined the Electronic Engineering Department of the same university, where he has been a Researcher from 1990 to 1998, a temporary Professor of Electromagnetics from 1994 to 1998, and an Associate Professor since 1998. His main research activity concerns guiding structures, antennas and resonators for microwaves and millimeter waves, numerical methods, scattering, optical propagation, plasma heating, and anisotropic media. Dr. Frezza is a Senior Member of IEEE, a Member of Sigma Xi, of AEI (Electrical and Electronic Italian Association), of SIOF (Italian Society of Optics and Photonics), of SIMAI (Italian Society for Industrial and Applied Mathematics), and of AIDAA (Italian Society of Aeronautics and Astronautics).

Massimo Santarsiero received *Laurea* degree in Physics in 1988 and Ph.D. degree in Applied Electromagnetics in 1992, from "La Sapienza" University of Rome. He worked at ENEA (Italian Energy and Environment Agency) on holography and interferometry. Presently he is at Department of Physics of the University "Roma Tre", where he works on optical coherence, laser beam characterization, electromagnetic scattering by microstructures.

Carlo Santini received the *Laurea* degree in Electronic Engineering in 1996 form "La Sapienza" University of Rome. He presently collaborates with the Department of Electronic Engineering of the same University on electromagnetic scattering problems. In 1997 he joined Telecom Halia and is now working in the strategic planning.

Giuseppe Schettini received the *Laurea* degree in Electronic Engineering in 1986, the Ph.D. degree in Applied Electromagnetics and Electrophysics Sciences in 1992, and the *Laurea* degree in Physics in 1995, all from "La Sapienza" University of Rome. After his gradua-

tion in Electronic Engineering he joined the ENEA (Italian Energy and Environment Agency) where he worked first on Free Electron Lasers, and then on the Radiofrequency heating of thermonuclear plasmas. In 1992 he joined "La Sapienza" University as Researcher and Assistant Professor of Electromagnetics. From 1995 to 1998 he has been a temporary Professor of Electromagnetic fields, and an Associate Professor since 1998. His scientific activity is focused on Radiofrequency heating of thermonuclear plasmas, Ferrite resonators, Propagation and diffraction of optical beams, Diffractive optics, Free electron lasers. Dr. Schettini is a member of the Italian Physical Society (SIF), Italian Optics and Photonics Society (SIOF), of the "La Sapienza" unit of the Electromagnetics Group of Italian National Research Council (CNR), and of the "La Sapienza" unit of the Electronics CNR Group.